



# Formation and Transformation of Iron Oxy-hydroxide Precursor Clusters to Ferrihydrite

Journal:	Environmental Science: Nano
Manuscript ID	EN-ART-12-2023-000930.R1
Article Type:	Paper

SCHOLARONE™ Manuscripts

## **Environmental Significance Statement**

Iron oxides and oxy-hydroxides are widely distributed across Earth's surface environments. Among these, ferrihydrite (Fh) has garnered substantial attention due to its small particle size and low structural order resulting in high specific surface area and high density of reactive surface sites of Fe nanoparticles. Therefore, Fh plays an essential role in sequestering contaminants and nutrients such as phosphate (PO<sub>4</sub><sup>3-)</sup> in natural environment. The formation of Fh is preceded by the precipitation of small oxy-hydroxide clusters during the rapid hydrolysis of Fe(III). Iron oxy-hydroxides with smaller particle sizes and greater structural disorder than Fh may exhibit a heightened affinity for interacting with ions and metals, such as through adsorption, before transitioning to Fh. The presence of other ions can stabilize metastable Fe oxy-hydroxide clusters, thereby impeding or delaying their transformation and growth to larger crystalline phases. These particles, being extremely small, can remain suspended, thereby increasing their mobility and potential to transport contaminants over longer distances, potentially impacting a larger area beyond their original source.

# Formation and Transformation of Iron Oxyhydroxide Precursor Clusters to Ferrihydrite

Alireza Namayandeh<sup>a,a\*</sup>, Olaf J. Borkiewicz<sup>b</sup>, Michel Sassi<sup>c</sup>, Kevin M. Rosso<sup>c</sup>, and F. Marc Michel<sup>a,e</sup>

<sup>a</sup> Department of Geosciences, Virginia Polytechnic Institute and State University, Blacksburg, VA 24061, USA

<sup>b</sup> Advanced Photon Source, Argonne National Laboratory, IL60439, USA

<sup>c</sup> Physical and Computational Sciences Directorate, Pacific Northwest National Laboratory, Richland, WA 99352, USA

<sup>d</sup> Department of Earth System Science, Stanford University, Stanford, CA 94305, USA

<sup>e</sup> Division of Nanoscience, Academy of Integrated Science, Virginia Polytechnic Institute and State University Blacksburg, VA 24061, USA

\*Email: arnama@stanford.edu

#### **Abstract**

Iron (Fe) oxy-hydroxide minerals such as ferrihydrite (Fh) are ubiquitous in Earth-surface environments and important in biogeochemical element cycling. Recent research has suggested that their formation is preceded by the precipitation of ultrasmall (~1 nm) Keggin-like Fe oxy-hydroxide clusters. However, relatively little is understood about the structure of the precursor clusters and the impacts of pH and time on their growth and transformation to more stable phases. We used a new method that involves mixed flow reactors (MFR) to synthesize these Fe oxy-hydroxide precursor clusters at pH 1.0, 1.5, 2.5, and 4.5. *In-situ* and *ex-situ* synchrotron scattering measurements and laboratory small-angle X-ray scattering (SAXS) were used to study

the structure and size of Fe oxy-hydroxide clusters and their transformation products, respectively. Results show that with increasing pH, the particle size and structural order of samples increase, forming solids that resemble 2-line Fh at pH 4.5. The experimental data were compared with X-ray pair distribution functions (PDF) calculated for a range of Fe(III) oxyhydroxide clusters, including Fe<sub>13</sub> Keggin isomers computed previously using density functional theory (DFT), which yielded at best only partial agreement at short range (< 5 Å). Aging of the clusters synthesized at pH 1.5 and 2.5 results in growth and transformation via Ostwald ripening to mixtures of goethite (Gt) and lepidocrocite (Lp). This process was inhibited by immediately reacting the early-formed clusters with phosphate ( $PO_4^{3-}$ ), suggesting that oxyanion surface complexes can stabilize the initial clusters by preventing growth and crystallization to more stable phases.

**Keywords**: Iron oxy-hydroxide clusters, Ferrihydrite, Fe<sub>13</sub> clusters, Goethite, Lepidocrocite, Aggregation, Pair distribution function analysis

### Introduction

Iron (Fe) oxides and oxy-hydroxides are widely distributed in Earth-surface environments and play significant roles in (bio)geochemical processes. <sup>1-7</sup> Among these, ferrihydrite (Fh) has received considerable attention due to its chemical reactivity and its status as a precursor to more thermodynamically stable phases. <sup>8-24</sup> Ferrihydrite can exist in various degrees of crystallinity, ranging from 2-line to 7-line Fh, <sup>2, 9, 25-28</sup> although samples with lower crystallinity than 2-line Fh have also been reported. <sup>2, 3, 29, 30</sup> These phases are metastable, undergoing transformation to more crystalline phases such as goethite (Gt), hematite (Hm), and lepidocrocite (Lp).<sup>8, 13, 31-35</sup> In addition, Fh, with its high adsorptive capacity, has a strong affinity for sequestering nutrients and contaminants in natural environment. <sup>12, 36-43</sup> The adsorption of other ions impacts the particle size and crystallinity of Fh, thereby controlling its nucleation, growth, and transformation. <sup>2, 3, 17, 31, 44-50</sup>

The formation of Fh is preceded by the precipitation of small oxy-hydroxide clusters during rapid Fe(III) hydrolysis, which can grow through aggregation to ultimately form Fh.  $^{20,51-55}$  A recent computational study  $^{52}$  proposed structures for a range of Fe oxy-hydroxide clusters, starting from a single hydrated Fe(III) ion that undergoes further hydrolysis to form low molecular weight Fe(III) dimers and trimers. The interaction of these species, through olation and oxolation, leads to the formation of larger oligomers such as Fe<sub>4</sub>, Fe<sub>5</sub>, and Fe<sub>7</sub>, as well as Fe<sub>13</sub> clusters known as Keggins (ions or clusters). Sadeghi et al.  $^{51}$  synthesized Fe<sub>13</sub> Keggin clusters (referred to as Fe<sub>13</sub> hereafter) confined in an anionic complex  $[FeO_4Fe_{12}F_{24}(OCH_3)_{12}]^{5-}$  and stabilized it using

countercations (Bi<sup>+3</sup>) and demonstrated that they serve as precursor clusters for the formation of Fh.

In a related study,  $^{20}$  an attempt was made to measure the size of Fe clusters precipitated at extremely acidic pH levels (<2) during Fe(III) hydrolysis, and it was concluded that an observed  $^{\sim}$  1.0 nm cluster is consistent with an Fe<sub>13</sub> Keggin surrounded by a Fe-depleted shell, a motif compatible with the structure of Fh. While these studies provided new insights into Fe oxyhydroxide clusters and their role in Fh formation, they primarily focused only on size,  $^{20}$  proxy structures,  $^{51}$  and computational analysis,  $^{52}$  without providing direct structural evidence.

In various natural environments, such as ferriferous seeps, mid-ocean ridge vents, and acid mine drainage (AMD) systems, Fe oxy-hydroxide clusters can interact with impurities, such as through adsorption, before evolving to Fh. <sup>2, 54</sup> The presence of other ions can stabilize metastable Fe oxy-hydroxides, thereby delaying or inhibiting their transformation. <sup>19, 44, 46-48, 56-58</sup> Iron oxy-hydroxides with smaller particle sizes and greater structural disorder than synthetic 2-line Fh have been observed in natural environments, often referred to as low crystalline 2-line Fh. <sup>2, 3, 29, 30</sup> Cismasu et al. <sup>3</sup> demonstrated that aluminum (AI), silica (Si), and natural organic matter (NOM) decreased the size and structural order of natural Fhs. They proposed that these impurities inhibited Fe polymerization and particle growth through complexation (Si and NOM) and cation substitution (AI). Other studies <sup>2, 30</sup> have shown that the sorption of oxyanions such as arsenate (AsO<sub>4</sub><sup>3-</sup>) and phosphate (PO<sub>4</sub><sup>3-</sup>) also had a similar impact on the formation of natural Fhs by reducing their size and the degree of structural order. It is worth noting that the formation of low crystalline Fh in aqueous environments is not exclusive to abiogenic Fh. Whitaker et al.<sup>29</sup>

reported the formation of poorly ordered biogenic Fh with a smaller coherent scattering domain size (CSD) compared to synthetic 2-line Fh. These studies have provided insights into the structure and size of natural Fhs, which may differ from those reported for 2-line Fh. It is reasonable to hypothesize that such low-ordered Fhs may consist of Fh precursors e.g., Fe<sub>13</sub> clusters, that have not yet evolved to Fh. Nevertheless, they are still commonly referred to as 2-line Fh, despite exhibiting significant differences in terms of reactivity and chemical behavior.

The synthesis and isolation of Fe oxy-hydroxide clusters in the laboratory pose challenges due to the rapid kinetics of Fe(III) hydrolysis reactions. <sup>20, 52-54, 59</sup> Previous studies have mainly employed base hydrolysis of Fe salts in batch reactors. <sup>20, 54, 60-63</sup> For instance, Zhu et al.<sup>54</sup> synthesized Fe oxy-hydroxide clusters by introducing NaHCO3 into a reactor containing ferric nitrate Fe(NO<sub>3</sub>)<sub>3</sub> solution. In another study, Weatherill et al. <sup>20</sup> conducted stirred batch reactor experiments by adding NaOH to acidified Fe(NO<sub>3</sub>) at different pH levels (0.5-9) to synthesize Fe oxy-hydroxide clusters. However, using batch reactors for synthesizing transient Fe oxyhydroxide clusters has certain disadvantages. These include: (1) the continuous addition of base leading to an increase in pH, resulting in a distribution of sizes and structural characteristics of the precipitates; (2) longer residence time for particles precipitated at the beginning of hydrolysis compared to those formed later; and (3) variation in ion supersaturation for particles formed at different pH levels and residence times. <sup>64</sup> An alternative method for synthesizing nanosized clusters under steady-state conditions is the mixed flow reactor (MFR), offering the advantage of precise control over residence time and solution chemistries. 64-67 This method can be easily adapted for different systems and combined with various in-situ characterization techniques. 66,

<sup>67</sup> Furthermore, the synthesized products can be collected, aged in batch reactors to examine growth or transformation behaviors, and prepared for *ex-situ* characterization. <sup>67</sup>

The present work focuses on investigating the formation of Fe oxy-hydroxide clusters and their transformation products. Our objective is to understand the influence of system chemistries on the size and structure of Fe oxy-hydroxide clusters and their role in Fh formation. We used a new method for synthesizing Fe oxy-hydroxide clusters and provided direct structural evidence of their formation and transformation. This new information is crucial for enhancing our understanding of the processes involved in the formation of Fe oxides and hydroxides in environmental systems.

## **Material and Methods**

Sample synthesis and *in-situ* SAXS. Known concentrations (0.03, 0.05, 0.1, and 0.3 M) of acidified  $Fe(NO_3)_3$  (ACS grade, Fisher Scientific) were prepared using ultra-pure (18.2 M $\Omega$ ) water in the background of 1 M HNO $_3$ . The initial solution was loaded in a 150 ml syringe and pumped into a stirred 5-mL mixed flow reactor (MFR) at 8 mL/min using a high-precision syringe pump (Harvard Apparatus PHD ULTRATM 4400). Simultaneously, a peristaltic pump (Ismatec Reglo ICC Digital Pump) was used to pump 2 M NaOH into MFR at different rates to obtain the selected target pHs (0.5, 1.0, 1.5, 2.5, 3.5, and 4.5) which were monitored in the effluent using an in-line pH probe. We excluded pH levels above 4.5 to prevent the formation of Fh and Gt. The residence time was ~30 seconds in all experiments. The resulting suspensions were passed through an *in-situ* laboratory small-angle x-ray scattering (SAXS) cell to measure particle size. SAXS data were collected using a laboratory Empyrean Nano Edition diffractometer system (Malvern-Panalytical)

equipped with a Cu source ( $\lambda K\alpha = 1.5406$  Å). The X-ray scattering cell for measuring the size of nanoparticle suspensions was a custom-designed 3D-printed flow cell (U.S. Patent Application No. 62/576,928) fabricated in the Michel lab at Virginia Tech. SAXS data were collected three times during each experiment. Subtraction of the background (DI water) and calculation of the volume-weighted size distribution (Dv(R)) was performed using EasySAXS software (Malvern-Panalytical).

In-situ synchrotron high-energy X-ray scattering. The same MFR experimental setup was used for conducting in-situ synchrotron high-energy total scattering measurements for pair distribution function (PDF) analysis. The experiments were performed at beamline 11-ID-B at the Advanced Photon Source (APS), Argonne National Laboratory. Acidified Fe(NO<sub>3</sub>)<sub>3</sub> solution with a concentration of 0.1 M and NaOH solution with a concentration of 2 M were continuously pumped into a stirred 5-mL MFR at different rates to achieve target pH values of 1.0, 1.5, 2.5, and 4.5. The resulting suspensions were then passed through the X-ray beam using a cylindrical 3 mm O.D. polyimide scattering cell. Data collection commenced once the pH stabilized and continued for approximately 20 minutes for each experiment. The background was prepared by adjusting the pH of a 1 M HNO<sub>3</sub> solution to match the target pH of each corresponding experiment using 2 M NaOH. The 2D detector images were converted into 1D two-theta vs. intensity and Q-space vs. intensity files using GSAS-II software <sup>68</sup>. Background subtraction and conversion of reciprocal data to real space data were conducted using xPDFsuite 69 with a maximum Q-space of 22-23 Å-1 for the Fourier transform. For more detailed information about the beamline setup and data processing, the reader should refer to the work by Hoeher et al. <sup>66</sup>

The sample PDFs were compared with reference data and calculated PDFs based on published structures. A reference 2-line Fh was synthesized using a modified version of Schwertmann and Cornell <sup>70</sup> to compare with the *in-situ* samples. The synthesis procedure and characterization of Fh have been described in Namayandeh et al. 2022. <sup>24</sup>

The PDFs of the samples were further compared with PDFs for a series of DFT-optimized structures using linear combination fitting (LCF). The details of the LCF method are provided in Text S1. Selected details for the DFT-optimized structures reported by Das<sup>52</sup> are given in Table S1. Although several of these LCF components have identical compositions and charges, they each have unique structural characteristics that result in distinct differences in the positions and intensities of correlations in the PDFs. As such, all of the components were used for LCF analysis. However, due to close similarities in the structures of the two Fe<sub>13</sub> Keggin ions, Fe<sub>13a</sub> and Fe<sub>13b</sub>, these were evaluated individually alongside the other components. The PDFs for the DFT-optimized structure models were calculated using DiffPy-CMI framework. <sup>71</sup> A Q<sub>max</sub> of 23 Å<sup>-1</sup> used for the Fourier Transform was the same as for the experimental PDF data. A dampening function was not used.

Ex-situ experiments. Samples synthesized at pH 1.0, 1.5, and 2.5 using the previously described MFR were subjected to aging in solution to investigate the changes in the size and structure of Fe oxy-hydroxides. The initial sample suspensions were transferred to 15 mL centrifuge tubes and aged in an incubator shaker at 25°C for different time points (0, 3, 5, 7, 10, 15, 21, 30 days). Three replicates were prepared for each time interval. Samples from each time interval were analyzed using laboratory SAXS and synchrotron PDF analyses. For the PDF analysis, the samples

were immediately frozen at -20°C until characterization at the APS. The data processing procedures for both experiments were identical to those used in the *in-situ* experiments.

A separate set of samples was synthesized at pH 1.5 to investigate the influence of  $PO_4^{3-}$  on the size and structure of the clusters during the aging process. The samples were transferred to 15 mL centrifuge tubes, and 5 mM of  $Na_2HPO_4$  was added. Subsequently, the adsorbed samples were aged in the incubator shaker at 25 °C for a period of up to 30 days. At the same time intervals as mentioned earlier, the samples were removed and subjected to analysis using SAXS.

### **Results and Discussion**

In-situ SAXS analysis. The volume-weighted size distribution of the samples was measured at different pH levels and initial Fe concentrations, [Fe]. For initial [Fe] of 0.05, 0.1, and 0.3 M, the size of samples increases from  $1.0 \pm 0.0$  to  $2.0 \pm 0.0$  nm,  $1.0 \pm 0.0$  to  $2.4 \pm 0.0$  nm, and  $1.2 \pm 0.0$  to  $2.5 \pm 0.1$  nm, respectively, as the pH increase from 0.5 to 4.5 (Fig. 1). Fig. S1 displays the measured SAXS profiles and the corresponding calculated size histograms, Dv(R).

Recent studies have reported the size of presumed Fe<sub>13</sub> to be ~1 nm,<sup>20, 51</sup> which is consistent with the measured size of particles synthesized in the MFR at pH 0.5 and 1.0 when using lower [Fe] (0.05 and 0.1 M). As the [Fe] and pH increase, more Fe precipitates during the hydrolysis process, <sup>8</sup> leading to the nucleation of larger particles. This suggests that Fe supersaturation plays an important role in controlling the sizes of the initially formed particles. At high supersaturation, the free energy barrier for particle nucleation is low, allowing particles to readily collide with each other in their intermediate vicinity and form larger particles through

Consequently, higher pH values promote particle attraction through van der Waals forces, causing small hydrolysis products to condensate and form larger aggregates. <sup>74, 76-79</sup> This observation aligns with the observed increase in particle size with pH in our study.

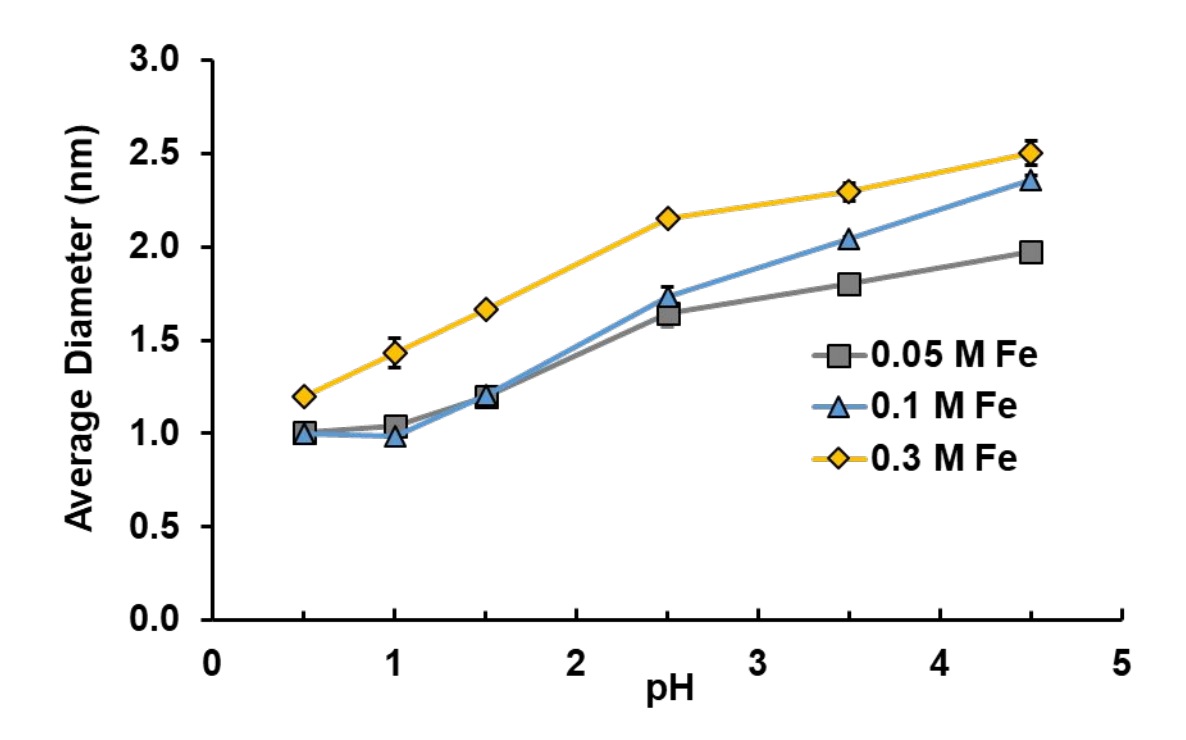


**Figure 1.** SAXS determined particle size across different pH and [Fe]. The error bars correspond to standard error (n=3). Error bars for some samples in these and other figures are smaller than the symbol.

In-situ total scattering and PDF analysis. *In-situ* total scattering and PDF analysis were used to investigate the structures and degree of structural order of the samples formed at pH 1.0, 1.5, 2.5, and 4.5, with a fixed [Fe] of 0.1 M. Figure 2a illustrates that the pH 1.0 sample exhibits a single prominent yet diffuse feature centered at  $Q \approx 2.35 \, \text{Å}^{-1}$ , which is lower than the reference Fh. With increasing pH, this feature became narrower and shifted to higher Q-values,

approaching the position of 2-line Fh. Concurrently, a broad feature centered at  $\sim 4.2 \, \text{Å}^{-1}$  emerges and increases in intensity, closely resembling the position of the second characteristic peak in 2-line Fh. The total scattering structure functions (Fig. 2b) display a similar trend towards 2-line Fh, while also exhibiting features at higher Q-space because the data being scaled as Q[S(Q)-1]. The amplification of the weaker intensity shows that the sample synthesized at pH 1.0 exhibits the least similarity to the 2-line Fh reference. The pH 4.5 sample shows the highest similarity; however, broader

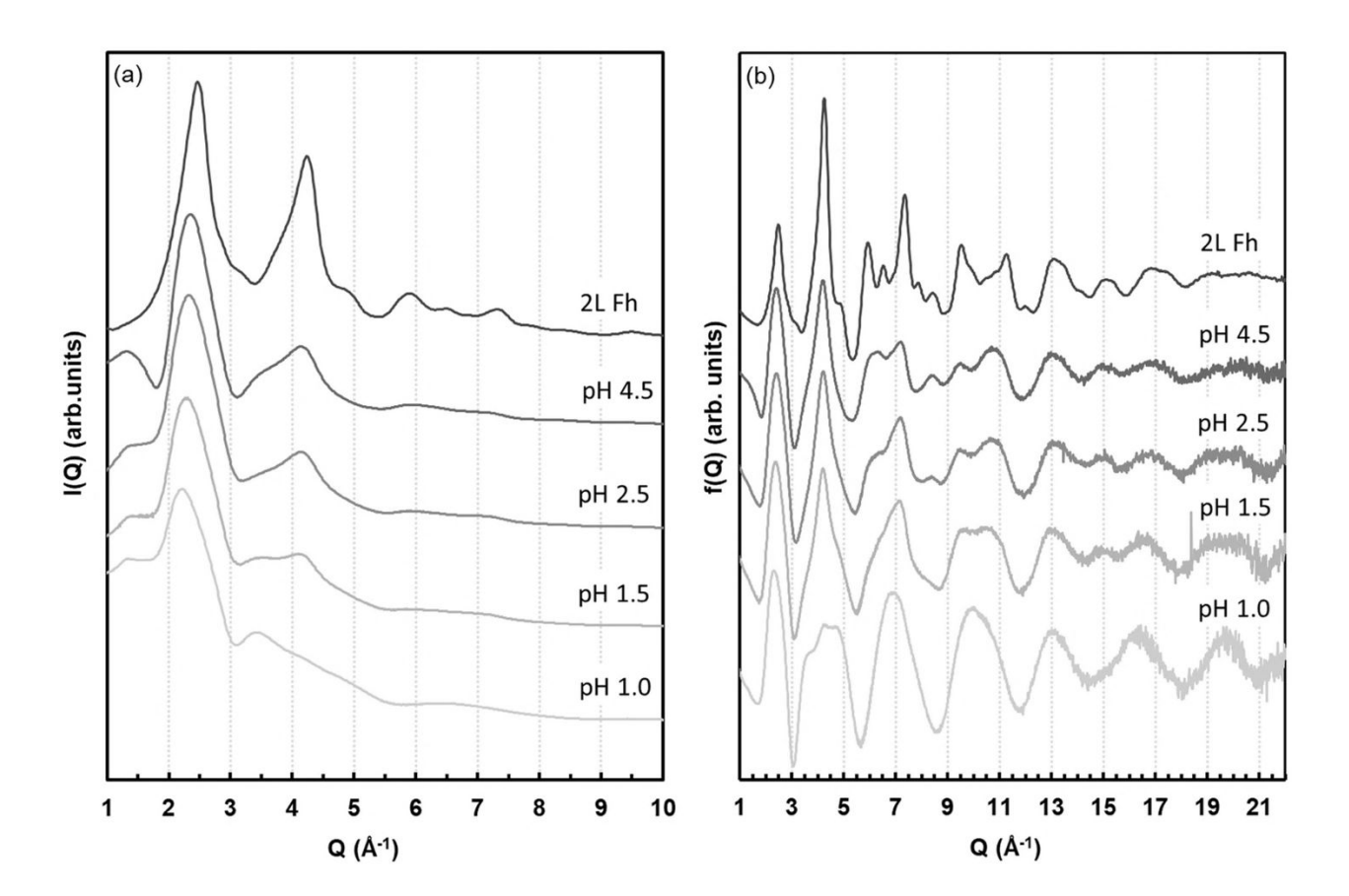


**Figure 2.** (a) Background-subtracted reciprocal-space intensity (I(Q)) for the *in situ* synthesis products formed at different pH compared with 2-line ferrihydrite. (b) Total scattering structure functions (f(Q)) for the same samples.

peak widths and intensity differences in the f(Q) data also indicate that the degree of structural order in this sample is lower than that of the 2-line Fh reference.

The PDFs provide information about the average short- to intermediate-range structures of the solids and allow for comparisons in the degree of structural order. <sup>2</sup> As shown in Fig. 3, the PDFs exhibit a smooth evolution towards 2-line Fh as pH increases, as evidenced by the positions and intensities of the correlations. The PDF for the reference 2-line Fh can be used to determine the atom pairs contributing to each correlation observed in the sample PDFs. For instance, the first

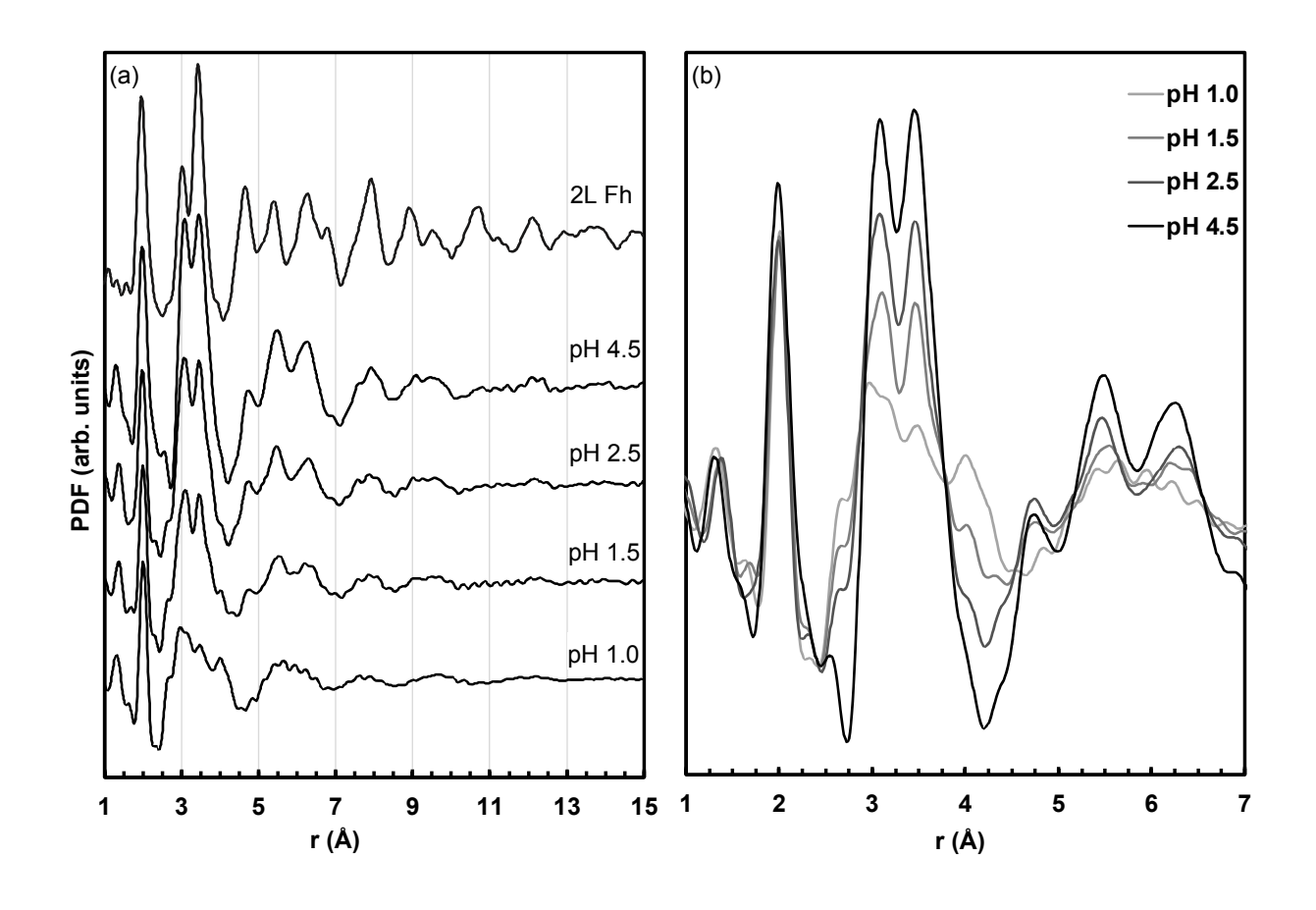


**Figure 3.** (a) PDFs for the *in-situ* synthesis products formed at different pH compared with 2-line ferrihydrite. (b) Overlay showing the evolution in the *in-situ* PDFs with increasing pH.

prominent correlation at ~ 2 Å in all samples corresponds with the average Fe-O bond length.  $^{52}$ ,  $^{80}$  The second and third strong correlations at ~ 3 and 3.5 Å, respectively, are mainly attributed to Fe...Fe pairs for FeO<sub>6</sub> octahedra in edge- and corner-sharing configurations. Additionally, correlations in this region of the PDFs may also involve tetrahedral Fe, FeO<sub>4</sub>, contributing to selected correlation in this region of the PDFs.  $^{28}$  Peaks at higher values of r generally involve multiple atom pairs, such as Fe...Fe, Fe...O, O...O, and have been previously assigned for Fh. $^{28}$ 

The PDF data demonstrate that the structural order of the *in-situ* samples becomes increasingly similar to 2-line Fh as the pH increases, but there are noticeable differences. One notable difference is the attenuation of the PDF correlations with increasing *r*, which can be used to estimate the CSD size. As shown in Fig. 3a, the CSD size of the *in-situ* samples is <10 Å, as indicated by the last visible correlation in the PDFs. In comparison, the estimated CSD size of the 2-line Fh reference is ~25 Å. The smaller CSD sizes in the *in-situ* samples could be attributed to the finite sizes of the particles (i.e., physical dimensions) or the lower structural order.

Another notable difference is the relative intensities of the features at ~3 and 3.5 Å, which are roughly one-to-one for the *in-situ* samples compared to one-to-two for the 2-line Fh reference. Furthermore, there is a distinct feature at ~4.8 Å dominated by Fe...O pairs, which increases with pH but remains suppressed relative to the reference. These differences may indicate variations in the connectivity of atoms within the structures, such as differences in the proportions of edge- and corner-sharing octahedra, or they could be attributed to reduced

particle size. <sup>28</sup> Lastly, the *in-situ* samples show a feature at  $\sim$  1.35 Å (Fig. 3b) that is not present in 2-line Fh. We assign this correlation to the average N-O bond length in nitrate (NO<sub>3</sub>-) <sup>53</sup> and attribute its presence to the minor residual background signal associated with nitric acid.

Synchrotron total scattering and laboratory SAXS data reveal that the average range of structural coherence (i.e., CSD size) and the physical dimensions (Dv(R) particle size) of the earlyformed hydrolysis products increase with increasing synthesis pH. Interestingly, at lower pH levels, the CSD sizes and Dv(R) sizes are similar, measuring approximately 1 nm or less. This observation suggests that the particles may be interpreted as ordered molecular clusters with finite sizes, rather than amorphous solids consisting of a continuous random network of atoms. However, as the pH increases, we observe a decoupling between the degree of structural order and particle size. For example, the CSD size of the pH 4.5 sample measures ~ 1.2 nm, whereas the SAXS particle size is double that, at ~ 2.4 nm. It is not possible to determine from these data alone whether the increase in particle size is due to aggregation or growth. Nevertheless, the PDFs indicate that the structures are becoming increasingly ordered with increasing pH. The results also suggest that the early-formed hydrolysis products at pH 4.5 are not yet well-formed 2-line Fh structures, indicating that the particles would need to continue growing to achieve increased intermediate-range structural order. Additional experiments are needed to determine what factors may contribute to the final evolution to 2-line Fh and may include bringing the samples to a higher pH, allowing them to further age, aggregate, settle, and/or dry.

Das<sup>52</sup> used computational molecular modeling at the DFT level of theory to explore Fe oxy-hydroxide cluster structures, including  $Fe_{13}$  Keggin structures, that are potentially incipient

to Fh. We compared calculated PDFs for a series of DFT-optimized structures from that study with the experimental PDFs for our *in-situ* samples using LCF. Figures S2, 3, 4, and 5 show comparisons of the *in-situ* sample to the calculated PDFs from Das<sup>52</sup>. LCF analysis of the experimental data using delta-Fe<sub>13a</sub> (#18) versus Fe<sub>13b</sub> (#19) revealed only minor differences; thus, we have chosen to focus on the results of fits using Fe<sub>13b</sub> in subsequent discussions. The L1-regression and combinatorial LCF analyses for samples synthesized at pH 1.0, 1.5, 2.5, and 4.5 yielded comparable outcomes. With the exception of pH 1.0, the analysis showed three components, Fe<sub>4b</sub> (#14), Fe<sub>7</sub> (#17), and Fe<sub>13b</sub> (#19), with significant weights. The results for the sample synthesized at pH 1.0 were significantly different in that this sample showed favored components Fe<sub>1</sub> (#1), Fe<sub>2f</sub> (#7), Fe<sub>3b</sub> (#10), Fe<sub>4b</sub> (#14), and Fe<sub>13b</sub> (#19), with Fe<sub>1</sub> the highest.

However, while LCF shows that various combinations of Das clusters can reproduce some of the features in the PDF data, the overall match quality remains unsatisfactory, as evident by the high residual from the LCF fit across all the pHs. The pH 4.5 sample was the most ordered of the *in-situ* samples and had a 10-12 Å CSD size consistent with Keggin clusters. <sup>51</sup> The DFT-optimized delta  $Fe_{13}$  Keggin structure exhibits the best match to the pH 4.5 sample in terms of the short-range structure <5 Å (Fig. 4a). However, differences in the structure at >5 Å are significant. Notably, there is an apparent absence of a correlation at ~ 6.75 Å, which involves both Fe...Fe and Fe...O pairs (Fig. 4b). Interestingly, the Fe...Fe pairs for this correlation correspond to the distances between the 12 Fe atoms on opposing sides of the  $Fe_{13}$  cluster. While the DFT-optimized  $Fe_{13}$  structure predicts the presence of this correlation, it is not detected in the *in-situ* samples synthesized in this work.

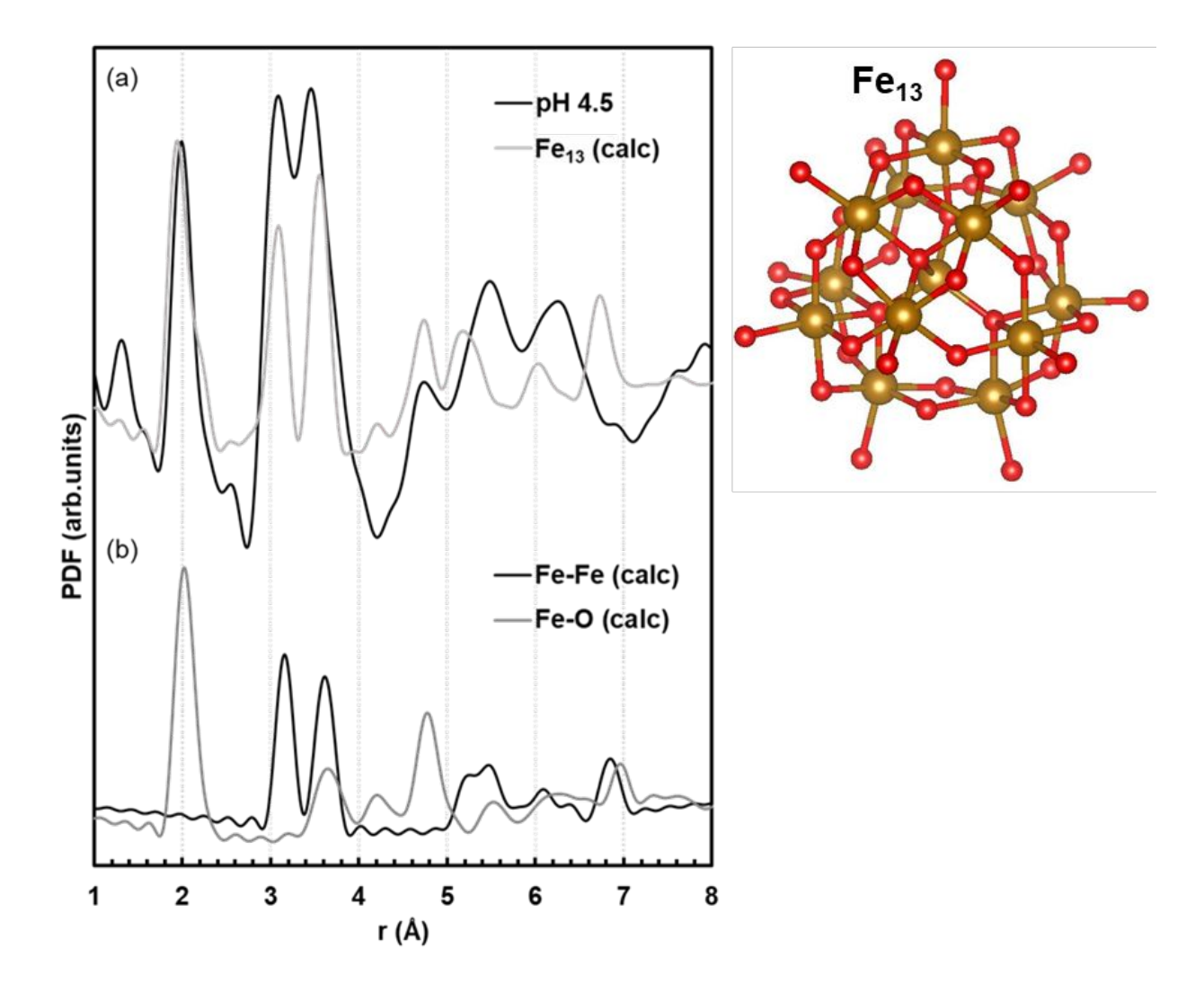


**Figure 4.** (a) PDF for the *in-situ* synthesis products formed at pH 4.5 compared with the calculated PDFs of the DFT-optimized structure for  $Fe_{13}$  reported by  $Das^{52}$  (b) Partial PDFs of contributing Fe-Fe and Fe-O in the structure of  $Fe_{13}$ . The PDF profile of  $Fe_{13}$  is normalized to the average Fe-O peak at ~ 2Å. The structural model for  $Fe_{13}$  is shown to the right of the PDF panel.

There are several possible explanations for the limited agreement between the *in-situ* experimental PDF and the DFT-derived structures. For instance, the experimental sample may not be a single, homogenous structure but instead a mixture of two or more different cluster structures. Das<sup>52</sup> predicted a range of Fe oxy-hydroxide clusters that may precipitate during the

rapid hydrolysis of Fe(III). They suggested that the formation of Fe<sub>13</sub> then proceeds through a gradual connection of dimeric oxy-hydroxide clusters, which may form stable trimeric, tetrameric, or oligomeric clusters such as Fe<sub>3</sub>, Fe<sub>4</sub>, Fe<sub>5</sub>, and Fe<sub>7</sub>. Due to the high reactivity of aqueous Fe(III) and the rapid kinetics of Fe oxy-hydroxide clusters reactions, it is possible that the simultaneous formation of these clusters or their rapid transformation into one another during synthesis under these conditions might be inevitable. Since the experimental PDF represents an average of all the different phases present in the sample, it would not be appropriate to use a single-phase model to describe a potentially multi-phase ensemble. 2, 81 However, this scenario is less likely because these clusters are very unstable, particularly at higher pHs, and will immediately transform to more stable structures. <sup>20, 52-54, 59</sup> Even in the case of a single-phase sample, it is necessary to have representative calculated structures for comparison with experimental data. Our current analysis is limited to the published structures obtained from Das,<sup>52</sup> which are derived from DFT energy minimizations performed on gas phase clusters; hence missing solvent effects could also be important. The LCF analysis showed that the Das<sup>52</sup> calculated structures are not sufficient for the identification of the structure(s) formed during our synthesis. Additional computational work is required to obtain representative geometries for the structures of different Fe oxy-hydroxide clusters in the aqueous phase.

Particle growth and transformation with aging. SAXS analysis shows differences in the average diameters of particles formed at pH 1.0, 1.5, and 2.5, as well as in the effects of aging the particles for up to 21 d (Fig. 5). Fig. S6 shows the measured SAXS profiles and calculated size histograms, Dv(R). As shown, the initial size of the samples precipitated at pH 1.0 and 1.5 are close to 1 nm, and raising the synthesis pH to 2.5 increased the initial size to ~1.8 nm. The size of particles grew

from  $1.2 \pm 0.0$  to  $3.0 \pm 0.1$  nm and  $1.8 \pm 0.1$  to  $3.2 \pm 0.1$  nm for samples pH 1.5 and 2.5, respectively, at steady state (i.e., after 10 days). Although the Fe supersaturation (0.1 M) remained constant for all the samples, less Fe precipitates during the hydrolysis at pH 1.0 compared to pH 1.5 and 2.5 due to increased solubility of Fe with decreasing pH. Higher solubility also enhances the critical nucleus size needed for the growth of particles  $^{72}$ . In addition, according to

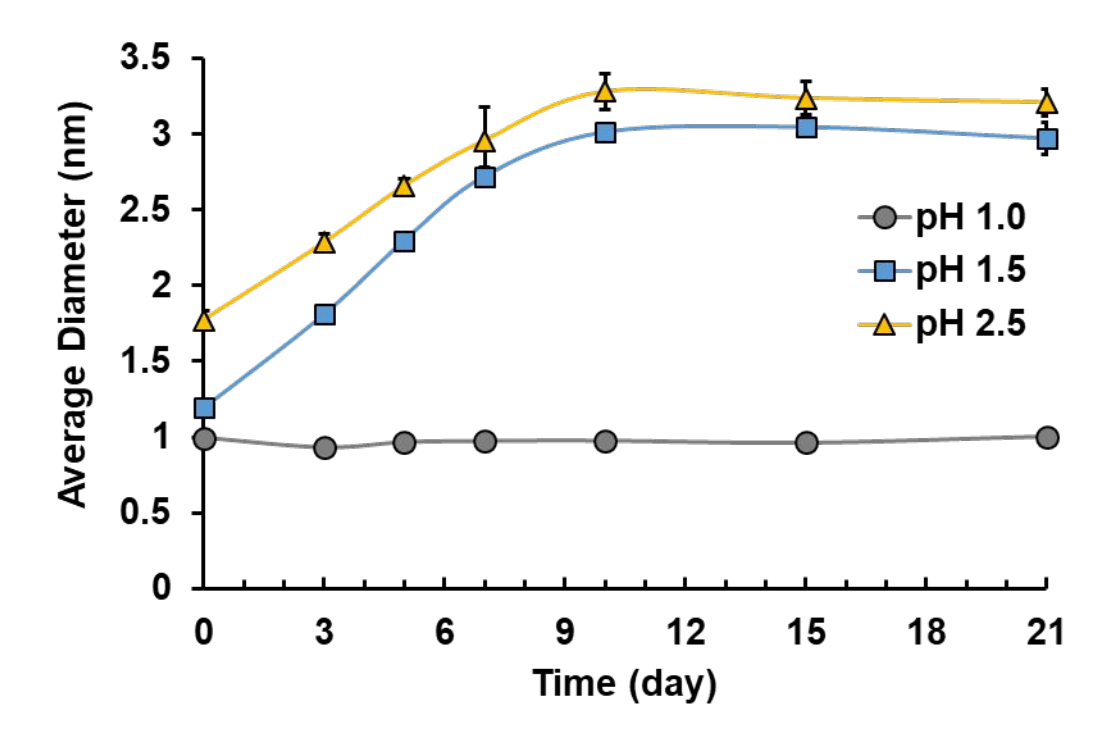


**Figure 5.** Determined size for the samples synthesized and aged at pH 1.0, 1.5, 2.5. The error bars correspond to standard error (n=3).

the Gibbs-Thomson relation, the solubility increases as the size of particles decreases, <sup>73</sup> which hinders the growth of particles with small radii of curvature. <sup>72</sup> Taken together, we attribute the lack of growth in the pH 1.0 samples to high solubility which results in the formation of small particle size (~ 1 nm) observed at this pH. Weatherill et al. <sup>20</sup> recently synthesized Fe oxy-

hydroxide clusters at pH 0.5 and 1.5 and reported that these samples remained persistent in solution for up to 18 days. The behavior of their pH 0.5 samples is consistent with our results. However, unlike our samples, their pH 1.5 samples also did not exhibit any growth. This lack of growth is attributed to the significantly lower initial [Fe] (0.0017 M) used in their experiment compared to the [Fe] (0.1 M Fe) used in this study.

We studied the particle growth mechanism at pH 1.5 and 2.5 using a rate model developed by Lifshitz, Slyzov, and Wagner. <sup>8, 82, 83</sup>

$$r^3 - r_0^3 = kt (1)$$

Where r is the particle radius at time t,  $r_0$  is the initial particle radius, and k is the rate constant. The plot of  $r^3$  versus t yields a straight line with the slope represented by k. This model describes diffusion-limited particle growth, where larger particles grow through the dissolution/recrystallization of smaller particles. This phenomenon is commonly known as Ostwald ripening. <sup>73</sup> Figure 6 illustrates the linear evaluation of  $r^3$  with time for pH 1.5 and 2.5, indicating that the dominant mechanism by which the particles grow is through the process of Ostwald ripening. The solubility and particle size are the most critical parameters controlling the mechanism of particle growth.<sup>72</sup> The likelihood that particles grow through the Ostwald ripening process, as opposed to aggregation through oriented attachment (OA), increases with increasing solubility and decreasing particle size. 72, 84, 85 In addition, at these pHs, the surface of particles exhibits high positive charges, resulting in the repulsion of particles, which is not favorable for the OA pathway. This is supported by the rate model analysis of our samples.

The samples synthesized and aged at pH 2.5 were selected and characterized using highenergy X-ray scattering to identify the crystalline products resulting from the transformation of Fe oxy-hydroxide clusters with aging (Fig. 7). The I(q) scattering data reveals that the broad peak at 2.3 Å<sup>-1</sup> shifts to 2.15 Å<sup>-1</sup> after 3 days. Additionally, a new broad peak emerges at 1.5 Å<sup>-1</sup> on day 7, which gradually develops into a sharper peak over time. Fifteen days after aging, multiple sharp and intense peaks emerge. These peaks were indexed with the known structure of several Fe oxy-hydroxide minerals, indicating the formation of Gt with a lesser amount of Lp as the products of transformation (Fig. 7). The formation of Gt through the transformation of Fe oxy-hydroxide

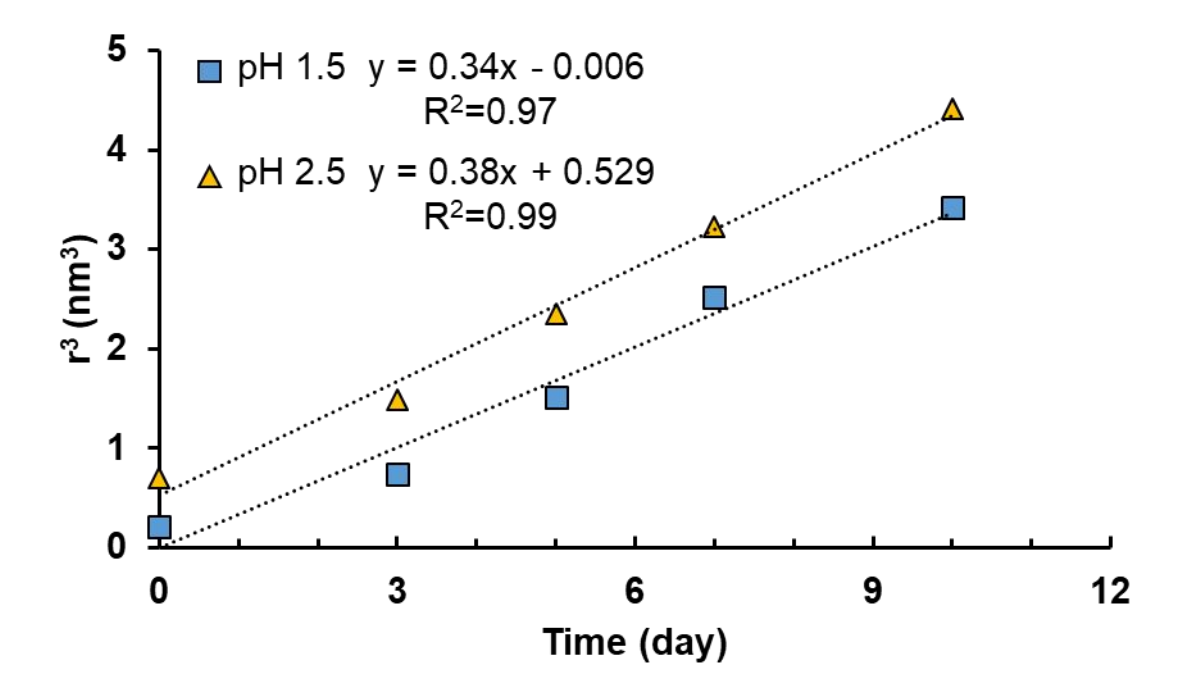


**Figure 6.** The plot of particle radius cubed (r³) versus time for samples synthesized at pH 1.5 and 2.5. Dashed lines represent linear fits determined by the method of least squares.

precursors such as Fh at acidic pH (less than  $\sim$  3) has been previously reported, with dissolution/recrystallization identified as the primary mechanism of transformation,  $^{32, 59, 86-88}$ 

which is consistent with the rate model analysis conducted in this work. In addition, the transformation occurred in the presence of  $NO_3^-$ , which has been reported to promote the formation of Gt through dissolution/recrystallization during the Fh transformation.<sup>24,89</sup> However, given the extremely acidic pH of the transformation, we posit pH was the primary controlling factor, and  $NO_3^-$  might not have had a significant influence. The *ex-situ* aged samples were frozen at -20  $^{\circ}$ C until characterization. Given that no crystalline phase was observed in samples on days 3 to 7, we believe freezing did not induce the formation of crystalline phases.

Although Fe oxy-hydroxide clusters are considered precursors to 2-line Fh, <sup>20, 51</sup> our samples appeared to undergo direct transformation to more stable phases, namely Gt and Lp. Iron oxy-hydroxide metastable phases are formed through rapid hydrolysis of Fe(III) solutions when their nucleation is kinetically favored. <sup>90</sup> However, they undergo transformation to thermodynamically stable phases during aging when there is sufficient time for crystallization. <sup>7, 19, 31, 32, 91-93</sup> In other words, the formation of a metastable phase through the transformation of another metastable phase is less likely, which aligns with the Ostwald ripening process that favors the formation of stable phases at the expense of metastable phases. <sup>8, 72, 73</sup>

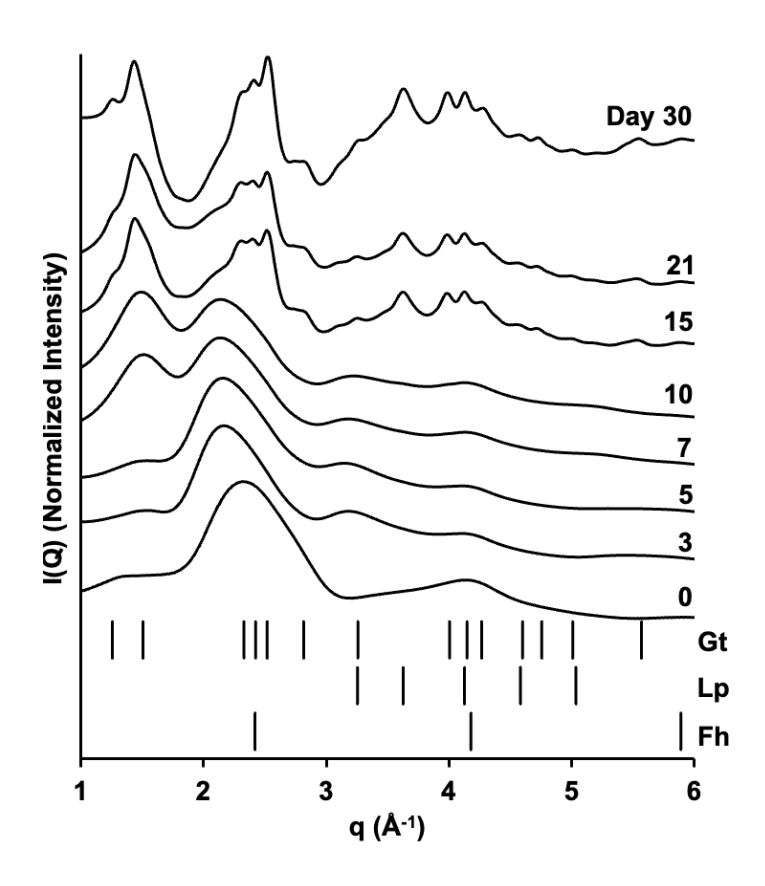


**Figure 7.** Normalized *I(q)* profiles for samples synthesized and aged at pH 2.5 for 30 days. Sample day 0 is the *in-situ* sample synthesized at pH 2.5. Ferrihydrite, goethite, and lepidocrocite tick marks were plotted based on their calculated X-ray diffraction patterns.

However, as the broad peaks of 2-line Fh can be suppressed in the presence of crystalline Gt and Lp in the I(q) profile, our data do not rule out minor formation of 2-line Fh with aging.

The *in-situ* experiments demonstrate that Fe oxy-hydroxide clusters have the potential to serve as precursors to 2-line Fh, but the aging experiments reveal that they do not transform into 2-line Fh at pH 2.5. Both *in-situ* and *ex-situ* experiments indicated that larger particles ( $^{\sim}$  2-3 nm) are required for the formation of either Fh or the stable phases Gt and Lp, respectively. However, in the *in-situ* experiments, the larger particles are formed during the nucleation process as a result of increasing pH and [Fe], whereas in the *ex-situ* experiments, the larger particles are

formed through growth during the aging process. This suggests that Fe oxy-hydroxide clusters are not exclusively precursor clusters for Fh; they can also serve as precursors to more stable phases such as Gt and Lp. During the rapid hydrolysis of Fe(III), Fe oxy-hydroxide clusters have the ability to polymerize and form 2-line Fh. However, if the thermodynamic conditions are not favorable for the formation of 2-line Fh, the metastable Fe oxy-hydroxide clusters may instead grow and transform into Gt and Lp. In the former process, the kinetics override the thermodynamics to favor the formation of 2-line Fh, whereas in the latter process, the thermodynamics play a more dominant role, leading to the formation of Gt and Lp.

Effect of  $PO_4^{3-}$ . The adsorption of  $PO_4^{3-}$  inhibited the growth of Fe clusters during aging. Figure 8 compares the size of  $PO_4^{3-}$ -adsorbed samples with the pH 1.5 samples. Despite both sets of samples being synthesized and aged at pH 1.5, the presence of  $PO_4^{3-}$  prevents particle growth and maintains sample stability during the aging process. In a recent study, we demonstrated that  $PO_4^{3-}$  adsorption can inhibit the transformation of Fh into Gt and Hm.  $^{94}$  Ligands such as  $PO_4^{3-}$  form strong inner-sphere complexes on the surface of Fe oxy-hydroxides,  $^{12, 37, 43, 94-99}$  displacing water and inhibiting particle dissolution required for the Ostwald ripening process.  $^{24, 90}$  Therefore, the adsorption of  $PO_4^{3-}$  stabilizes Fe oxy-hydroxide clusters by suppressing their particle growth and transformation, as evidenced by the consistent size of the  $PO_4^{3-}$ -adsorbed samples during aging (Fig. 8).

In this work, we used  $PO_4^{3-}$  as a proxy to investigate the influence of surface impurities on the particle growth of Fe oxy-hydroxide clusters.

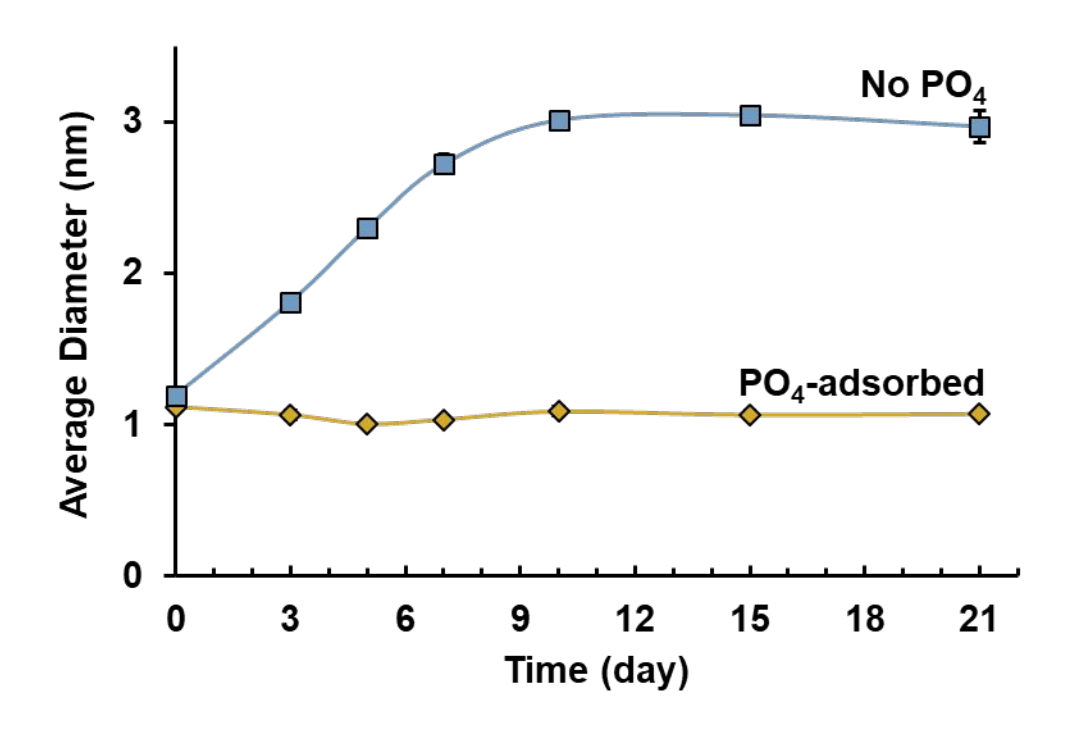


**Figure 8.** The variation in the particle size with time in the presence and absence of phosphate. Both sets of samples were synthesized at pH 1.5. The error bars correspond to standard error (n=3).

Previous studies <sup>2, 29, 49, 50, 100</sup> have reported that natural Fhs exhibit smaller particle sizes and greater structural disorder compared to synthetic 2-line Fh. <sup>2, 3, 29, 30</sup> These studies attributed the smaller particle sizes and increased structural disorder of natural Fh to the presence of impurities such as AsO<sub>4</sub><sup>3-</sup>, <sup>2, 49</sup> PO<sub>4</sub><sup>3-</sup>, <sup>50</sup> and NOM <sup>100</sup> during the nucleation and growth of Fh, which aligns with the impact of PO<sub>4</sub><sup>3-</sup> observed in our samples. A recent study <sup>94</sup> showed that the impact of PO<sub>4</sub><sup>3-</sup> and AsO<sub>4</sub><sup>3-</sup> on the rate and pathway of Fh transformation is comparable, which was attributed to their similar type and strength of inner-sphere complexation on the Fh surface. The adsorption of these ions can dehydrate the surface of Fe oxyhydroxide clusters, significantly decrease the dissolution, and, therefore, recrystallization of crystalline products. In addition, by occupying the interface between Fe particles, they can suppress the aggregation pathway, thereby hindering growth. This suggests that the reported small and structurally disordered

natural Fhs may actually correspond to clusters of Fe oxy-hydroxide that are stabilized by impurities. The inhibition of particle growth can have significant implications for the transportation of nutrients and contaminants in aqueous environments. Due to their extremely small size, these particles can remain suspended, thereby increasing their mobility in aquatic environments and allowing them to be transported over longer distances. Consequently, contaminants adsorbed onto these colloidal particles can be transported farther from their original source, potentially impacting a larger area. Additional characterizations of natural Fe oxy-hydroxide samples are required to identify their structure by comparing them with synthetic samples and computational models.

### Conclusion

This work demonstrates the influence of system chemistry on the size and structure of Fe oxy-hydroxide clusters. We have shown that the particle size increases with higher Fe supersaturation and pH. Our *in-situ* PDF analysis reveals that the structural order and CSD size increase with pH, resulting in the formation of solids resembling 2-line Fh at pH 4.5. While the samples exhibit significant similarities with the DFT-optimized structure of delta-Fe<sub>13</sub>, some differences in the intermediate range order of their structures are observed. These differences may be attributed to the presence of other Fe oxy-hydroxide clusters alongside Fe<sub>13</sub> in our samples. Additionally, gas phase DFT structures may not be the true representative of the clusters formed in water.

Collectively, our findings provide direct structural evidence for the formation of Fh from Fe oxy-hydroxide clusters. The *ex-situ* experiments reveal that samples synthesized at pH 1.0

were stable for up to 30 days, while the particle size for samples pH 1.5 and 2.5 increases with aging, leading to the formation of Gt and Lp as the transformed products. Our kinetic model suggests that dissolution/recrystallization is the predominant mechanism driving particle growth and transformation. We propose that during aging, thermodynamics become dominant over kinetics, favoring the formation of thermodynamically stable phases.

Furthermore, SAXS analysis demonstrates that the presence of PO<sub>4</sub><sup>3-</sup> inhibits particle growth, suggesting that impurities can stabilize Fe oxy-hydroxide clusters in natural environments. This work introduces a novel method for synthesizing Fe oxy-hydroxide clusters and provides direct structural evidence for their formation and transformation. We anticipate that these findings have implications for understanding the processes of Fe oxide and oxy-hydroxide formation in environmental systems.

#### **Author Contributions**

Alireza Namayandeh: conceptualization, methodology, investigation, visualization, formal analysis, and writing — original draft. Olaf J. Borkiewicz: investigation, formal Analysis, and methodology. Michel Sassi: investigation, formal analysis, methodology, and writing — review & editing. Kevin M. Rosso: investigation, formal analysis, and writing — review & editing. F. Marc Michel: conceptualization, methodology, investigation, formal analysis, writing — review & editing, funding acquisition, and supervision.

#### **Conflicts of interest**

There are no conflicts to declare.

### **Acknowledgments**

FMM gratefully acknowledges the financial support provided by the National Science Foundation through CAREER-1652237 and the Virginia Tech National Center for Earth and Environmental Nanotechnology Infrastructure ("NanoEarth", NSF Cooperative Agreement 1542100). Also, this research was partly funded by the Geological Society of America Graduate Student Research Grant. KMR and MS gratefully acknowledge support from the U.S. Department of Energy, Office of Science, Office of Basic Energy Sciences, Chemical Sciences, Geosciences, and Biosciences Division, through its Geosciences program at Pacific Northwest National Laboratory (FWP 56674). This research used resources of the Advanced Photon Source, a U.S. Department of Energy (DOE) Office of Science User Facility operated for the DOE Office of Science by Argonne National Laboratory under Contract No. DE-AC02-06CH11357.

#### References

- 1. Jambor, J. L.; Dutrizac, J. E., Occurrence and Constitution of Natural and Synthetic Ferrihydrite, a Widespread Iron Oxyhydroxide. *Chemical Reviews* **1998**, *98* (7), 2549-2586.
- 2. Michel, F. M., Total Scattering Studies of Natural and Synthetic Ferrihydrite. In *Advanced Applications of Synchrotron Radiation in Clay Science*, Clay Minerals Society: 2014; Vol. 19, p 0.
- 3. Cismasu, A. C.; Michel, F. M.; Tcaciuc, A. P.; Tyliszczak, T.; Brown, J. G. E., Composition and structural aspects of naturally occurring ferrihydrite. *Comptes Rendus Geoscience* **2011**, *343* (2), 210-218.
- 4. Cornell, R. M.; Schwertmann, U., *The iron oxides : structure, properties, reactions, occurences and uses.* 2., compl. rev. and ext. ed. ed.; Wiley-VCH: Weinheim :, 2003.
- 5. Hochella, M. F.; Lower, S. K.; Maurice, P. A.; Penn, R. L.; Sahai, N.; Sparks, D. L.; Twining, B. S., Nanominerals, Mineral Nanoparticles, and Earth Systems. *Science* **2008**, *319* (5870), 1631.
- 6. Hochella Jr, M. F.; Mogk, D. W.; Ranville, J.; Allen, I. C.; Luther, G. W.; Marr, L. C.; McGrail, B. P.; Murayama, M.; Qafoku, N. P.; Rosso, K. M. J. S., Natural, incidental, and engineered nanomaterials and their impacts on the Earth system. **2019**, *363* (6434), eaau8299.
- 7. Schoepfer, V. A.; Burton, E. D., Schwertmannite: A review of its occurrence, formation, structure, stability and interactions with oxyanions. *Earth-Science Reviews* **2021**, *221*, 103811.
- 8. Burleson, D. J.; Penn, R. L., Two-step growth of goethite from ferrihydrite. *Langmuir* **2006**, *22* (1), 402-409.
- 9. Michel, F. M.; Ehm, L.; Antao, S. M.; Lee, P. L.; Chupas, P. J.; Liu, G.; Strongin, D. R.; Schoonen, M. A. A.; Phillips, B. L.; Parise, J. B., The Structure of Ferrihydrite, a Nanocrystalline Material. *Science* **2007**, *316* (5832), 1726.
- 10. Borch, T.; Masue, Y.; Kukkadapu, R. K.; Fendorf, S., Phosphate Imposed Limitations on Biological Reduction and Alteration of Ferrihydrite. *Environmental Science & Technology* **2007**, *41* (1), 166-172.

- 11. Hiemstra, T.; Riemsdijk, W. H. V.; Rossberg, A.; Ulrich, K.-U., A surface structural model for ferrihydrite II: Adsorption of uranyl and carbonate. *Geochimica et Cosmochimica Acta* **2009**, *73* (15), 4437-4451.
- 12. Antelo, J.; Fiol, S.; Pérez, C.; Mariño, S.; Arce, F.; Gondar, D.; López, R., Analysis of phosphate adsorption onto ferrihydrite using the CD-MUSIC model. *Journal of Colloid and Interface Science* **2010**, 347 (1), 112-119.
- 13. Das, S.; Hendry, M. J.; Essilfie-Dughan, J., Transformation of two-line ferrihydrite to goethite and hematite as a function of pH and temperature. *Environmental science & technology* **2011**, *45* (1), 268-275.
- 14. Cismasu, A. C.; Michel, F. M.; Stebbins, J. F.; Levard, C.; Brown Jr, G. E., Properties of impurity-bearing ferrihydrite I. Effects of Al content and precipitation rate on the structure of 2-line ferrihydrite. *Geochimica et Cosmochimica Acta* **2012**, *92*, 275-291.
- 15. Hiemstra, T., Surface and mineral structure of ferrihydrite. *Geochimica et Cosmochimica Acta* **2013,** *105*, 316-325.
- 16. Zhu, M.; Northrup, P.; Shi, C.; Billinge, S. J.; Sparks, D. L.; Waychunas, G. A., Structure of sulfate adsorption complexes on ferrihydrite. *Environ. Sci. Technol. Lett.* **2013**, *1* (1), 97.
- 17. Michael Bolanz, R.; Bläss, U.; Ackermann, S.; Ciobotă, V.; Rösch, P.; Tarcea, N.; Popp, J.; Majzlan, J. J. C.; Minerals, C., The effect of antimonate, arsenate, and phosphate on the transformation of ferrihydrite to goethite, hematite, feroxyhyte, and tripuhyite. *Clays and Clay Minerals* **2013**, *61* (1), 11-25.
- 18. Adra, A.; Morin, G.; Ona-Nguema, G.; Brest, J., Arsenate and arsenite adsorption onto Alcontaining ferrihydrites. Implications for arsenic immobilization after neutralization of acid mine drainage. *Appl. Geochem.* **2015**, *64*, 2.
- 19. Soltis, J. A.; Feinberg, J. M.; Gilbert, B.; Penn, R. L., Phase Transformation and Particle-Mediated Growth in the Formation of Hematite from 2-Line Ferrihydrite. *Crystal Growth & Design* **2016**, *16* (2), 922-932.
- 20. Weatherill, J. S.; Morris, K.; Bots, P.; Stawski, T. M.; Janssen, A.; Abrahamsen, L.; Blackham, R.; Shaw, S., Ferrihydrite formation: the role of Fe13 Keggin clusters. *Environmental science & technology* **2016**, *50* (17), 9333-9342.
- 21. Namayandeh, A.; Kabengi, N., Calorimetric study of the influence of aluminum substitution in ferrihydrite on sulfate adsorption and reversibility. *Journal of Colloid and Interface Science* **2019**, *540*, 20-29.
- 22. Aeppli, M.; Kaegi, R.; Kretzschmar, R.; Voegelin, A.; Hofstetter, T. B.; Sander, M. J. E. s.; technology, Electrochemical analysis of changes in iron oxide reducibility during abiotic ferrihydrite transformation into goethite and magnetite. **2019**, *53* (7), 3568-3578.
- 23. Sassi, M.; Rosso, K. M., Ab Initio Evaluation of Solid-State Transformation Pathways from Ferrihydrite to Goethite. *ACS Earth and Space Chemistry* **2022**, *6* (3), 800-809.
- 24. Namayandeh, A.; Borkiewicz, O. J.; Bompoti, N. M.; Chrysochoou, M.; Michel, F. M., Oxyanion Surface Complexes Control the Kinetics and Pathway of Ferrihydrite Transformation to Goethite and Hematite. *Environmental Science & Technology* **2022**, *56* (22), 15672-15684.
- 25. Jansen, E.; Kyek, A.; Schäfer, W.; Schwertmann, U., The structure of six-line ferrihydrite. *Applied Physics A* **2002**, *74* (1), s1004-s1006.
- 26. Kukkadapu, R. K.; Zachara, J. M.; Fredrickson, J. K.; Smith, S. C.; Dohnalkova, A. C.; Russell, C. K., Transformation of 2-line ferrihydrite to 6-line ferrihydrite under oxic and anoxic conditions. *American Mineralogist* **2003**, *88* (11-12), 1903-1914.
- 27. Rancourt, D. G.; Meunier, J. F., Constraints on structural models of ferrihydrite as a nanocrystalline material. *American Mineralogist* **2008**, *93* (8-9), 1412.

- 28. Michel, F. M.; Barrón, V.; Torrent, J.; Morales, M. P.; Serna, C. J.; Boily, J. F.; Liu, Q.; Ambrosini, A.; Cismasu, A. C.; Brown, G. E., Ordered ferrimagnetic form of ferrihydrite reveals links among structure, composition, and magnetism. *Proc. Natl. Acad. Sci. U. S. A.* **2010**, *107* (7), 2787.
- 29. Whitaker, A. H.; Austin, R. E.; Holden, K. L.; Jones, J. L.; Michel, F. M.; Peak, D.; Thompson, A.; Duckworth, O. W., The structure of natural biogenic iron (oxyhydr)oxides formed in circumneutral pH environments. *Geochimica et Cosmochimica Acta* **2021**, *308*, 237-255.
- 30. Majzlan, J.; Lalinská, B.; Chovan, M.; Bläß, U.; Brecht, B. r.; Göttlicher, J. r.; Steininger, R.; Hug, K.; Ziegler, S.; Gescher, J., A mineralogical, geochemical, and microbiogical assessment of the antimony- and arsenic-rich neutral mine drainage tailings near Pezinok, Slovakia. *American Mineralogist* **2011,** *96* (1), 1-13.
- 31. Johnston, J. H.; Lewis, D. G., A detailed study of the transformation of ferrihydrite to hematite in an aqueous medium at 92°C. *Geochimica et Cosmochimica Acta* **1983**, *47* (11), 1823-1831.
- 32. Schwertmann, U.; Stanjek, H.; Becher, H. H., Long-term in vitro transformation of 2-line ferrihydrite to goethite/hematite at 4, 10, 15 and 25°C. *Clay Minerals* **2004**, *39* (4), 433-438.
- 33. Stemig, A. M.; Do, T. A.; Yuwono, V. M.; Arnold, W. A.; Penn, R. L., Goethite nanoparticle aggregation: effects of buffers, metal ions, and 4-chloronitrobenzene reduction. *Environmental Science: Nano* **2014**, *1* (5), 478-487.
- 34. Sheng, A.; Liu, J.; Li, X.; Qafoku, O.; Collins, R. N.; Jones, A. M.; Pearce, C. I.; Wang, C.; Ni, J.; Lu, A.; Rosso, K. M., Labile Fe(III) from sorbed Fe(II) oxidation is the key intermediate in Fe(II)-catalyzed ferrihydrite transformation. *Geochimica et Cosmochimica Acta* **2020**, *272*, 105-120.
- 35. Hansel, C. M.; Benner, S. G.; Fendorf, S., Competing Fe(II)-Induced Mineralization Pathways of Ferrihydrite. *Environmental Science & Technology* **2005**, *39* (18), 7147-7153.
- 36. Fendorf, S.; Eick, M. J.; Grossl, P.; Sparks, D. L., Arsenate and chromate retention mechanisms on goethite. 1. Surface structure. *Environ. Sci. Technol.* **1997**, *31* (2), 315.
- 37. Arai, Y.; Sparks, D. L., ATR–FTIR Spectroscopic Investigation on Phosphate Adsorption Mechanisms at the Ferrihydrite–Water Interface. *Journal of Colloid and Interface Science* **2001,** *241* (2), 317-326.
- 38. Sparks, D. L., *Environmental soil chemistry*. 2nd ed., ed.; San Diego, Calif.: London: Academic: San Diego, Calif.: London, 2003.
- 39. Sparks, D. L., Fundamentals of Soil Chemistry. *Encyclopedia of Water: Science, Technology, and Society* **2019**, 1-11.
- 40. Sposito, G., The Chemistry of Soils. Oxford University Press: New York:, 1987.
- 41. Sposito, G., The chemistry of soils. 2nd ed ed.; Oxford University Press: Oxford, 2008.
- 42. Elzinga, E. J.; Kretzschmar, R., In situ ATR-FTIR spectroscopic analysis of the co-adsorption of orthophosphate and Cd(II) onto hematite. *Geochimica et Cosmochimica Acta* **2013**, *117*, 53-64.
- 43. Antelo, J.; Arce, F.; Fiol, S., Arsenate and phosphate adsorption on ferrihydrite nanoparticles. Synergetic interaction with calcium ions. *Chemical Geology* **2015**, *410*, 53-62.
- 44. Das, S.; Hendry, M. J.; Essilfie-Dughan, J., Effects of adsorbed arsenate on the rate of transformation of 2-line ferrihydrite at pH 10. *Environmental science & technology* **2011**, *45* (13), 5557-5563.
- 45. Das, S.; Essilfie-Dughan, J.; Hendry, M. J. J. C. G., Fate of adsorbed arsenate during phase transformation of ferrihydrite in the presence of gypsum and alkaline conditions. **2015**, *411*, 69-80.
- 46. Lu, Y.; Hu, S.; Wang, Z.; Ding, Y.; Lu, G.; Lin, Z.; Dang, Z.; Shi, Z., Ferrihydrite transformation under the impact of humic acid and Pb: kinetics, nanoscale mechanisms, and implications for C and Pb dynamics. *Environmental Science: Nano* **2019**, *6* (3), 747-762.
- 47. Jones, A. M.; Collins, R. N.; Rose, J.; Waite, T. D., The effect of silica and natural organic matter on the Fe(II)-catalysed transformation and reactivity of Fe(III) minerals. *Geochimica et Cosmochimica Acta* **2009**, *73* (15), 4409-4422.

- 48. Zhang, D.; Wang, S.; Wang, Y.; Gomez, M. A.; Duan, Y.; Jia, Y., The transformation of two-line ferrihydrite into crystalline products: effect of pH and media (sulfate versus nitrate). *ACS Earth and Space Chemistry* **2018**, *2* (6), 577-587.
- 49. Waychunas, G. A.; Rea, B. A.; Fuller, C. C.; Davis, J. A., Surface chemistry of ferrihydrite: Part 1. EXAFS studies of the geometry of coprecipitated and adsorbed arsenate. *Geochimica et Cosmochimica Acta* **1993**, *57* (10), 2251-2269.
- 50. Rose, J.; Flank, A.-M.; Masion, A.; Bottero, J.-Y.; Elmerich, P., Nucleation and Growth Mechanisms of Fe Oxyhydroxide in the Presence of PO4 Ions. 2. P K-Edge EXAFS Study. *Langmuir* **1997**, *13* (6), 1827-1834.
- 51. Sadeghi, O.; Zakharov, L. N.; Nyman, M., Aqueous formation and manipulation of the iron-oxo Keggin ion. *Science* **2015**, *347* (6228), 1359-1362.
- 52. Das, B., Theoretical Study of Small Iron—Oxyhydroxide Clusters and Formation of Ferrihydrite. *The Journal of Physical Chemistry A* **2018**, *122* (2), 652-661.
- 53. Zhang, H.; Waychunas, G. A.; Banfield, J. F., Molecular Dynamics Simulation Study of the Early Stages of Nucleation of Iron Oxyhydroxide Nanoparticles in Aqueous Solutions. *The Journal of Physical Chemistry B* **2015**, *119* (33), 10630-10642.
- 54. Zhu, M.; Frandsen, C.; Wallace, A. F.; Legg, B.; Khalid, S.; Zhang, H.; Mørup, S.; Banfield, J. F.; Waychunas, G. A., Precipitation pathways for ferrihydrite formation in acidic solutions. *Geochim. Cosmochim. Acta* **2016**, *172*, 247.
- 55. Banfield, J. F.; Welch, S. A.; Zhang, H.; Ebert, T. T.; Penn, R. L., Aggregation-based crystal growth and microstructure development in natural iron oxyhydroxide biomineralization products. *Science* **2000**, *289* (5480), 751-754.
- 56. Hu, S.; Lu, Y.; Peng, L.; Wang, P.; Zhu, M.; Dohnalkova, A. C.; Chen, H.; Lin, Z.; Dang, Z.; Shi, Z., Coupled kinetics of ferrihydrite transformation and As (V) sequestration under the effect of humic acids: a mechanistic and quantitative study. *Environmental science & technology* **2018**, *52* (20), 11632-11641.
- 57. Shimizu, M.; Zhou, J.; Schröder, C.; Obst, M.; Kappler, A.; Borch, T., Dissimilatory reduction and transformation of ferrihydrite-humic acid coprecipitates. *Environmental science & technology* **2013**, *47* (23), 13375-13384.
- 58. ThomasArrigo, L. K.; Kaegi, R.; Kretzschmar, R., Ferrihydrite Growth and Transformation in the Presence of Ferrous Iron and Model Organic Ligands. *Environmental science & technology* **2019**, *53* (23), 13636-13647.
- 59. Jolivet, J.-P.; Chanéac, C.; Tronc, E., Iron oxide chemistry. From molecular clusters to extended solid networks. *Chemical Communications* **2004**, (5), 481-483.
- 60. Zhu, M.; Legg, B.; Zhang, H.; Gilbert, B.; Ren, Y.; Banfield, J. F.; Waychunas, G. A., Early-stage formation of iron oxyhydroxides during neutralization of simulated acid mine drainage solutions. *Environ. Sci. Technol.* **2012**, *46* (15), 8140.
- 61. Vilgé-Ritter, A.; Rose, J.; Masion, A.; Bottero, J. Y.; Lainé, J. M., Chemistry and structure of aggregates formed with Fe-salts and natural organic matter. *Colloids and Surfaces A: Physicochemical and Engineering Aspects* **1999**, *147* (3), 297-308.
- 62. Collins, R. N.; Rosso, K. M.; Rose, A. L.; Glover, C. J.; David Waite, T., An in situ XAS study of ferric iron hydrolysis and precipitation in the presence of perchlorate, nitrate, chloride and sulfate. *Geochimica et Cosmochimica Acta* **2016**, *177*, 150-169.
- 63. Rose, J.; Manceau, A.; Masion, A.; Bottero, J.-Y., Structure and Mechanisms of Formation of FeOOH(NO3) Oligomers in the Early Stages of Hydrolysis. *Langmuir* **1997**, *13* (12), 3240-3246.
- 64. Blue, C. R.; Rimstidt, J. D.; Dove, P. M., Chapter Twenty-Three A Mixed Flow Reactor Method to Synthesize Amorphous Calcium Carbonate Under Controlled Chemical Conditions. In *Methods in Enzymology*, De Yoreo, J. J., Ed. Academic Press: 2013; Vol. 532, pp 557-568.

- 65. Blue, C. R.; Giuffre, A.; Mergelsberg, S.; Han, N.; De Yoreo, J. J.; Dove, P. M., Chemical and physical controls on the transformation of amorphous calcium carbonate into crystalline CaCO3 polymorphs. *Geochimica et Cosmochimica Acta* **2017**, *196*, 179-196.
- 66. Hoeher, A.; Mergelsberg, S.; Borkiewicz, O. J.; Dove, P. M.; Michel, F. M., A new method for in situ structural investigations of nano-sized amorphous and crystalline materials using mixed-flow reactors. *Acta Crystallographica Section A* **2019**, *75* (5), 758-765.
- 67. Hoeher, A. J.; Mergelsberg, S. T.; Borkiewicz, O. J.; Michel, F. M., Impacts of Initial Ca/P on Amorphous Calcium Phosphate. *Crystal Growth & Design* **2021**, *21* (7), 3736-3745.
- 68. Toby, B. H.; Von Dreele, R. B., GSAS-II: the genesis of a modern open-source all purpose crystallography software package. *Journal of Applied Crystallography* **2013**, *46* (2), 544-549.
- 69. Yang, X.; Juhas, P.; Farrow, C. L.; Billinge, S. J., xPDFsuite: an end-to-end software solution for high throughput pair distribution function transformation, visualization and analysis. *arXiv: Materials Science* **2014**.
- 70. Schwertmann, U.; Cornell, R. M., *Iron oxides in the laboratory : preparation and characterization*. 2nd completely rev. and extended ed. ed.; Wiley-VCH: Weinheim ;, 2000.
- 71. Juhas, P.; Farrow, C. L.; Yang, X.; Knox, K. R.; Billinge, S. J. L., Complex modeling: a strategy and software program for combining multiple information sources to solve ill posed structure and nanostructure inverse problems. *Acta Crystallographica Section A* **2015**, *71* (6), 562-568.
- 72. De Yoreo, J. J.; Gilbert, P. U.; Sommerdijk, N. A.; Penn, R. L.; Whitelam, S.; Joester, D.; Zhang, H.; Rimer, J. D.; Navrotsky, A.; Banfield, J. F. J. S., Crystallization by particle attachment in synthetic, biogenic, and geologic environments. **2015**, *349* (6247), aaa6760.
- 73. Voorhees, P. W., The theory of Ostwald ripening. *Journal of Statistical Physics* **1985**, *38* (1), 231-252.
- 74. Butler, J. A. V., Theory of the Stability of Lyophobic Colloids. *Nature* **1948**, *162* (4113), 315-316.
- 75. Derjaguin, B.; Landau, L. J. Z. E. I. T. F., Theory of stability of highly charged liophobic sols and adhesion of highly charged particles in solutions of electrolytes. **1945**, *15* (11), 663-682.
- 76. Elimelech, M.; Gregory, J.; Jia, X., *Particle deposition and aggregation: measurement, modelling and simulation*. Butterworth-Heinemann: 2013.
- 77. Penn, R. L.; Tanaka, K.; Erbs, J., Size dependent kinetics of oriented aggregation. *Journal of Crystal Growth* **2007**, *309* (1), 97-102.
- 78. Burrows, N. D.; Hale, C. R. H.; Penn, R. L., Effect of pH on the Kinetics of Crystal Growth by Oriented Aggregation. *Crystal Growth & Design* **2013**, *13* (8), 3396-3403.
- 79. Derjaguin, B. V.; Landau, L. D., Theory of the stability of strongly charged lyophobic sols and of the adhesion of strongly charged particles in solutions of electrolytes. *Acta physicochim URSS* **1941**, *14*, 633–662.
- 80. Bottero, J. Y.; Manceau, A.; Villieras, F.; Tchoubar, D. J. L., Structure and mechanisms of formation of iron oxide hydroxide (chloride) polymers. **1994**, *10* (1), 316-319.
- 81. Chapter 3 The method of total scattering and atomic pair distribution function analysis. In *Pergamon Materials Series*, Egami, T.; Billinge, S. J. L., Eds. Pergamon: 2003; Vol. 7, pp 55-99.
- 82. Lifshitz, I. M.; Slyozov, V. V., The kinetics of precipitation from supersaturated solid solutions. *Journal of Physics and Chemistry of Solids* **1961,** *19* (1), 35-50.
- 83. Wagner, C., Theorie der Alterung von Neiderschlagen durch Umlosen (Ostwald Reifung): Zeitschrift Elektrochemica, v. 65. **1961**.
- 84. Lupulescu, A. I.; Rimer, J. D. J. S., In situ imaging of silicalite-1 surface growth reveals the mechanism of crystallization. **2014**, *344* (6185), 729-732.
- 85. Li, D.; Nielsen, M. H.; Lee, J. R. I.; Frandsen, C.; Banfield, J. F.; De Yoreo, J. J., Direction-Specific Interactions Control Crystal Growth by Oriented Attachment. *Science* **2012**, *336* (6084), 1014-1018.

- 86. Cudennec, Y.; Lecerf, A., The transformation of ferrihydrite into goethite or hematite, revisited. *Journal of Solid State Chemistry* **2006**, *179* (3), 716-722.
- 87. Schwertmann, U. B. B. R. D.; Cornell, R. M., Iron oxides in the laboratory preparation and characterization. Second, completely rev. and extended ed. ed.; Wiley-VCH: Weinheim:, 2000. Volltext <a href="http://sfx.ethz.ch/sfx">http://sfx.ethz.ch/sfx</a> locater?sid=ALEPH:EBI01&genre=book&isbn=9783527296699.
- 88. Mackay, A. In *Some aspects of the topochemistry of the iron oxides and hydroxides*, Reactivity of solids: Proceedings of the fourth international symposium on the reactivity of solids, 1960; pp 571-583.
- 89. Namayandeh, A.; Zhang, W.; Watson, S. K.; Borkiewicz, O. J.; Bompoti, N. M.; Chrysochoou, M.; Penn, R. L.; Michel, F. M., Goethite and Hematite Nucleation and Growth from Ferrihydrite: Effects of Oxyanion Surface Complexes. *Environmental Science & Technology* **2024**.
- 90. Schwertmann, U.; Cornell, R. M., Iron Oxides in the Laboratory. Wiley: New York 2008.
- 91. Fischer, W.; Schwertmann, U. J. C. C. M., The formation of hematite from amorphous ir on (iii) hydroxide. **1974**, *23*, 33-37.
- 92. Jönsson, J.; Persson, P.; Sjöberg, S.; Lövgren, L., Schwertmannite precipitated from acid mine drainage: phase transformation, sulphate release and surface properties. *Appl. Geochem.* **2005**, *20* (1), 179.
- 93. Vithana, C. L.; Sullivan, L. A.; Burton, E. D.; Bush, R. T., Stability of schwertmannite and jarosite in an acidic landscape: Prolonged field incubation. *Geoderma* **2015**, *239-240*, 47-57.
- 94. Namayandeh, A.; Borkiewicz, O. J.; Bompoti, N. M.; Watson, S. K.; Kubicki, J. D.; Chrysochoou, M.; Michel, F. M., Effects of Oxyanion Surface Loading on the Rate and Pathway of Ferrihydrite Transformation. *ACS Earth and Space Chemistry* **2023**, *7* (10), 2154-2165.
- 95. Geelhoed, J. S.; Hiemstra, T.; Van Riemsdijk, W. H., Phosphate and sulfate adsorption on goethite: Single anion and competitive adsorption. *Geochimica et Cosmochimica Acta* **1997**, *61* (12), 2389-2396.
- 96. Hongshao, Z.; Stanforth, R. J. E. S.; Technology, Competitive adsorption of phosphate and arsenate on goethite. **2001**, *35* (24), 4753-4757.
- 97. Carabante, I.; Grahn, M.; Holmgren, A.; Hedlund, J., In situ ATR–FTIR studies on the competitive adsorption of arsenate and phosphate on ferrihydrite. *Journal of Colloid and Interface Science* **2010**, *351* (2), 523-531.
- 98. Kubicki, J. D.; Paul, K. W.; Kabalan, L.; Zhu, Q.; Mrozik, M. K.; Aryanpour, M.; Pierre-Louis, A. M.; Strongin, D. R., ATR–FTIR and Density Functional Theory Study of the Structures, Energetics, and Vibrational Spectra of Phosphate Adsorbed onto Goethite. *Langmuir* **2012**, *28* (41), 14573.
- 99. Zhang, X.; Yao, H.; Lei, X.; Lian, Q.; Roy, A.; Doucet, D.; Yan, H.; Zappi, M. E.; Gang, D. D., A comparative study for phosphate adsorption on amorphous FeOOH and goethite ( $\alpha$ -FeOOH): An investigation of relationship between the surface chemistry and structure. *Environmental Research* **2021,** *199*, 111223.
- 100. Mikutta, C., X-ray absorption spectroscopy study on the effect of hydroxybenzoic acids on the formation and structure of ferrihydrite. *Geochimica et Cosmochimica Acta* **2011**, *75* (18), 5122-5139.

# Data availability statement

The data supporting this article have been included as part of the Supplementary Information.